

Microbubble clustering in turbulent flow

Enrico Calzavarini ^{*},¹ Thomas H. van den Berg,¹ Federico Toschi,² and Detlef Lohse¹

¹*Department of Applied Physics, University of Twente, 7500 AE Enschede, The Netherlands.*

²*IAC-CNR, Istituto per le Applicazioni del Calcolo, Viale del Policlinico 137,
I-00161 Roma, Italy and INFN, via Saragat 1, I-44100 Ferrara, Italy.*

(Dated: February 9, 2020)

Single-point hot-wire measurements in the bulk of a turbulent channel have been performed in order to detect and quantify the phenomenon of preferential bubble accumulation. We show that statistical analysis of the bubble-probe colliding-times series can give a robust method for investigation of clustering in the bulk regions of a turbulent flow where, due to the opacity of the flow, no imaging technique can be employed. We demonstrate that microbubbles ($R_0 \simeq 100 \mu\text{m}$) in a developed turbulent flow, where the Kolmogorov length-scale is $\eta \simeq R_0$, display preferential concentration in small scale structures with a typical statistical signature ranging from the dissipative range, $\mathcal{O}(\eta)$, up to the low inertial range $\mathcal{O}(100\eta)$. A comparison with Eulerian-Lagrangian numerical simulations is also presented to further support our proposed way to characterize clustering from temporal time series.

PACS numbers: 47.55.Kf, 47.27.T-

INTRODUCTION

The phenomenon of preferential concentration of small particles and bubbles in turbulent flows attracted much attention in recent years, from experimental works [1], to numerical investigations [2, 3, 4, 5] and theory developments, [6, 7]. The preferential accumulation may be understood as an inertial effect. Due to inertia the Lagrangian particle/bubble velocity is not always aligned with the surrounding incompressible fluid flow velocity and this leads to the consequence that particles heavier than the fluid are on average ejected from vortices, while light buoyant particles tend to accumulate in high vorticity regions.

The scenario is complicated by the fact that a certain number of other physical effects may play a role. First, apart from body forces like gravity and added mass, there are in general surface forces acting on the particles, as for example drag and lift, whose expressions especially in unsteady flow conditions are not completely understood. For a discussions on the dynamics of a single particle settling in still fluid and for the rise of a single bubble we refer to [8, 9, 10, 11]. Such forces may in principle produce additional non trivial effects on the clustering mechanism. Secondly, the coupling of the disperse phase on the fluid flow (*two-way* coupling) and the finite-size effect of particle-particle interaction (*4-way* coupling) may also result in non-negligible factors of perturbation for preferential concentration of particles in highly turbulent flows.

Small air bubbles in water, below the millimeter size, i.e. of typical Reynolds number of order $\mathcal{O}(1)$, can be re-

garded as a particular kind of non-deformable light spherical particles with density negligibly small compared to the fluid one. In fact, in this size-range, shape oscillations or deformations and wake induced effect can be reasonably neglected. Strong preferential accumulation in core vortex regions is therefore expected according to the inertia mechanism, see for instance the experimental visualizations realized by Douady *et al.* [12]. An explorative experimental investigation on the relevant features of microbubbles clustering in a developed turbulent flow is the focus of the present paper.

Experimental measurements on bubbly laden turbulent flows are challenging. Even at very low void fractions ($\sim 1\%$) the fluid tends to be completely opaque and difficult, if not impossible, to access with external optical methods, especially in the bulk region of the flow. Recently, we have performed a series of experiments in order to understand the effect of bubbles, [13], and microbubbles, [14], on the turbulent energy spectra. Numerics based on Eulerian-Lagrangian description also have been successfully employed to predict the same effects in similar flow conditions, [15, 16]. In particular, it has been demonstrated that for low void fractions, up to few percents, microbubbles induce an energy decrease at large scales and an energy enhancement at small scales. For these kind of experiments, where the main focus was on fluid velocity, a traditional *intrusive* hot-wire anemometer has been adopted, the disturbances associated to bubbles hitting the probe were successively identified and filtered out when computing fluid turbulent spectra, [17, 18].

One could object that measurement from one fixed point in space are too intrusive because they can destroy the clusters, or that they are ineffective in extracting features of the bubble trapping in turbulent vortical structures. However, in this paper we analyze the series of

^{*}Electronic adress: e.calzavarini@tnw.utwente.nl

the bubble colliding times on the hot-wire probe from the Twente experiment by means of appropriate statistical indicators. We show that it is possible to detect and quantify the micro-bubble clustering from a one-point measurement set-up. We compare experimental findings with results from numerical simulations based on Eulerian-Lagrangian approach. Due to limitations that we will discuss later, at best only a qualitative agreement among numerics and experiments is expected. Nevertheless, we show how this comparison is helpful in clarifying the trend in the clustering at changing the turbulent conditions.

DETAILS OF THE EXPERIMENT METHODS

The experimental set-up, as previously mentioned, is the Twente water channel, a vertical duct of square cross section with dimension $200\text{cm} \times 45\text{cm} \times 45\text{cm}$, we refer to Rensen *et al.* [13] for a detailed description. An array of porous ceramic plates, positioned on the top of the channel, is used to generate co-flowing small bubbles of average radius, $R_0 \simeq 100\mu\text{m}$, as described in [14]. Fluid turbulence is generated by means of an active grid, positioned immediately downstream the bubble injection sites. The typical flow is characterized by a large mean flow, U , with turbulent fluctuations, $u' \equiv \langle (u_z(t) - U)^2 \rangle_t^{1/2}$, of smaller amplitude. The condition $u'/U \ll 1$ assures that Taylor's frozen-flow hypothesis can be applied. The dissipative Kolmogorov scale measures typically $\eta = 400 \div 500 \mu\text{m}$, while the Taylor micro-scale and the integral one, are respectively $\lambda \simeq 30 \eta$, and $L_0 \simeq 500 \eta$. The typical bubble size is of the same order, or weakly smaller, than η .

We consider microbubble signals extracted from a hot-film anemometry probe ($300 \mu\text{m}$ in size) fixed at the center of the channel. Detection of micro-bubbles is luckily less ambiguous than for large bubbles where probe piercing and break-up events are highly probable [19]. A micro-bubble hitting the probe produces a signal with a clear spike and the bubble can be identified by threshold check on the velocity time-derivative signal, see Fig. 1. This identification procedure leads to the definition of a minimal cut-off time in the capability to detect clustered events, two consecutive bubbles in our records cannot have a separation time smaller than $\tau = 10^{-2}\text{sec}$. Such dead-time is mainly linked to the typical response-time of the acquisition set-up. Here we consider two time series of microbubble measurements, i.e. hitting times, selected from a larger database because of their uniformity and relevant statistics, we will refer to them in the following as sample (a) and (b). The first sample (a) has been taken for a 12 hours long measurement; it consists of $N_b = 24099$ bubbles with a mean hitting frequency $f = 0.56 \text{ sec}^{-1}$. The second sample, (b), is a record of 11 hours, $N_b = 11194$ and $f \simeq 0.28 \text{ sec}^{-1}$. There

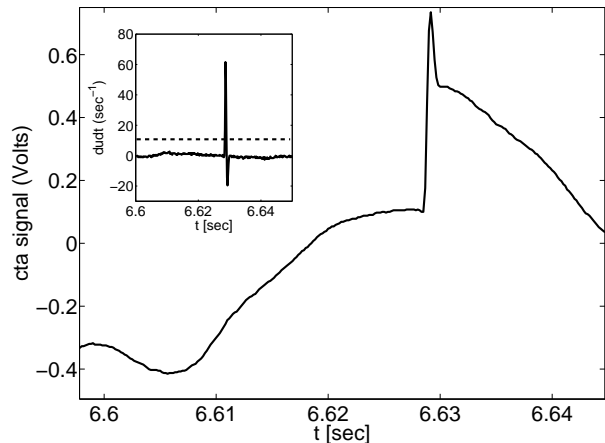


FIG. 1: A typical voltage, $V(t)$, signal from the hot-wire anemometer, a spike is produced by a hitting micro-bubble. Due to the internal electrical impedance of the acquiring set-up we consider the signal's perturbation fully restored after 10^{-2} sec . The inset shows for the same event, the voltage time derivative normalized by the mean velocity standard deviation ($dudt$). The dotted line shows the level of the threshold adopted for bubble identifications.

are two main differences among the experimental conditions in which the two samples have been recorded, that is the total volume air fraction (called void fraction α), and the amplitude of the mean flow and therefore the intensity of turbulence. Case (a) has a void fraction of $\approx 0.3\%$ and (b) has instead $\alpha \approx 0.1\%$. Note that, even at these very small void fractions, the mean number density of bubbles amounts to $O(10^2)$ per cubic centimeter, this explains the optical opacity of the bulk region of our system. Nevertheless, given the small effect produced by the dispersed bubbly phase on the turbulent cascading mechanism, [14], we consider the discrepancy in α as irrelevant for the velocity spectra. In contrast, the difference in the forcing amplitude is more important, because it changes sensibly all the relevant scales of turbulence as summarized in Table I. In particular, this leads to different values for the minimal experimentally detectable scale: $\Delta r_{min} \simeq 5\eta$ for case (a) and $\Delta r_{min} \simeq 3\eta$ for (b), where Taylor hypothesis has been used to convert time to space measurements, i.e. $\Delta r = \tau \cdot U$. In the following, results of our analysis will be presented by adopting space units made dimensionless by the Kolmogorov scale η , we consider this re-scaling more useful for comparison with different experiments and simulations where a mean flow may be absent.

	L_0 (cm)	U (cm/s)	u' (cm/s)	Re_λ	τ_{eddy} (s)	τ_η (ms)	η (μm)	u_η (mm/s)	Re_b	R_0/η	St	$g\tau_b/u_\eta$
a)	22.6	19.4	1.88	206	12.0	151.	388.	2.57	4.4	0.26	0.007	4.2
b)	23.1	14.2	1.39	180	16.6	240.	489.	2.04	4.4	0.20	0.004	5.3

TABLE I: Relevant turbulent scales and bubble characteristics for the two experimental samples analyzed. Fluid turbulent quantities have been estimated from one-dimensional energy spectra. From left to right: integral scale, L_0 , mean velocity, U , single-component root mean square velocity, u' , Taylor Reynolds number, Re_λ , large eddy turnover time, τ_{eddy} , dissipative time (τ_η) space (η) and velocity (u_η) scales, bubble Reynolds number, Re_b , bubble-radius and Kolmogorov-length ratio, R_0/η , Stokes number, St , ratio between terminal velocity in still fluid and dissipative velocity scale, $g\tau_b/u_\eta$.

DESCRIPTION OF THE STATISTICAL TOOLS

In this section we introduce the statistical tests that we will adopt to quantify the clustering. Due to the fact that the experimental recording is a temporal series of events, we have necessarily to focus on a tool capable to identify, from within this one dimensional serie, possible signatures of 3D inhomogeneities.

A first way to assess the presence of preferential concentrations in the experimental records is to compute the probability density function (pdf) of the distance, Δr , between two consecutive bubbles. Whether the particles distribute homogeneously in space, their distribution would be a Poissonian distribution and hence the distance between two consecutive bubbles would be given by the well know exponential expression: $\rho \exp(-\rho \Delta r)$, where $\rho = f/U$ is the number of bubbles per unit length (i.e. their density) [20]. Due to the presence of turbulence we expect that in general the spatial location of bubble will differ from a Poissonian distribution: in any case it is natural to expect that for separation-scales large enough the exponential form of the pdf should be recovered. In fact, pairs of successive bubbles with large separations Δr , larger then any structures in the flow, are expected to be uncorrelated, memory-less, events.

Due to the possible accumulation on small scales (clustering of bubbles) the long tail of the pdf may have an exponential decay rate that is different from the global mean, ρ . The tail of the experimentally measured pdf can be fitted with an exponentially decaying function, $A \cdot \exp(-\rho_h \Delta r)$, with a rate that we call ρ_h , where h stands for homogeneous. In case of small-scale clustering we expect ρ_h to be smaller than ρ . As an indicator of the fraction of bubbles accumulated in turbulent structures, we use the coefficient $\mathcal{C} \equiv 1 - \rho_h/\rho$, whose value varies in between 0 and 1.

The test so far introduced is useful but provides only an indication on how much the space distribution of bubbles is or not homogeneous at small scales while gives no particular indications on their possible ‘‘large-scale’’ correlations. Here we introduce a second, more comprehensive, statistical test particularly convenient to reveal the scales at which the inhomogeneity starts to take place. The idea is to compute the coarse-grained

central moments of the number of bubbles, on a window of variable length r , $\mu_r^p \equiv \langle (n - \langle n \rangle_r)^p \rangle_r$. The length of the window r will be the scale at which we study if or not the distribution resembles or deviate from an homogeneous one. We will focus on scale dependent Kurtosis and Skewness excesses, respectively: $K(r) \equiv \mu_r^4/(\mu_r^2)^2 - 3$ and $S(r) \equiv \mu_r^3/(\mu_r^2)^{3/2}$. A random distribution of particles spatially homogeneous with mean density ρ would corresponds to the Poissonian distribution : $p(n) = \exp(-\rho r)(\rho r)^n (n!)^{-1}$, where r is the length of the spatial window and n is the number of expected events. Therefore, once the particle space rate ρ is given, the value of any statistical moments and their combinations can be derived for the corresponding window length r . A spatially Poissonian distribution of particles implies the functional dependences $K(r) = (\rho r)^{-1}$ and $S(r) = (\rho r)^{-1/2}$. Furthermore, we note that at the smallest scale, when $r = \Delta r_{min}$, we reach the singular limit (shot-noise limit) where for any given space-window we can find only 0 or 1 bubbles and all statistical moments collapse to the same value. This latter limit, which is by the way coincident with Poisson statistics, represents our minimal detectable scale. We are interested in departures from the shot-noise/random-homogeneous behavior for the statistical observables $K(r)$ and $S(r)$.

RESULTS OF THE ANALYSIS ON EXPERIMENTAL DATA

In figure 2 we show the computed pdf(Δr) for the two data samples considered. Deviations from global homogeneity are clear if the shape of the histogram is compared with the solid line representing the pdf $\rho \exp(-\rho \Delta r)$. These deviations are weakly more marked in case (a), the most turbulent, than case (b). Nevertheless, one can notice that the pure exponentially decaying behavior, i.e. homogeneity, is recovered from distances of the order of $\mathcal{O}(100\eta)$ up to the large scales. The dotted line on Fig. 2, which represents the linear fit on the long homogeneous tail in the interval $[10^3, 2 \cdot 10^3]\eta$, and the inset boxes, where the pdf is compensated by the fit, shows this latter feature. The evaluation of the coefficient \mathcal{C} leads to values for the relative bubbles excess in clusters corresponding to 19 % for case (a) ($Re_\lambda \simeq 206$) and 10 %

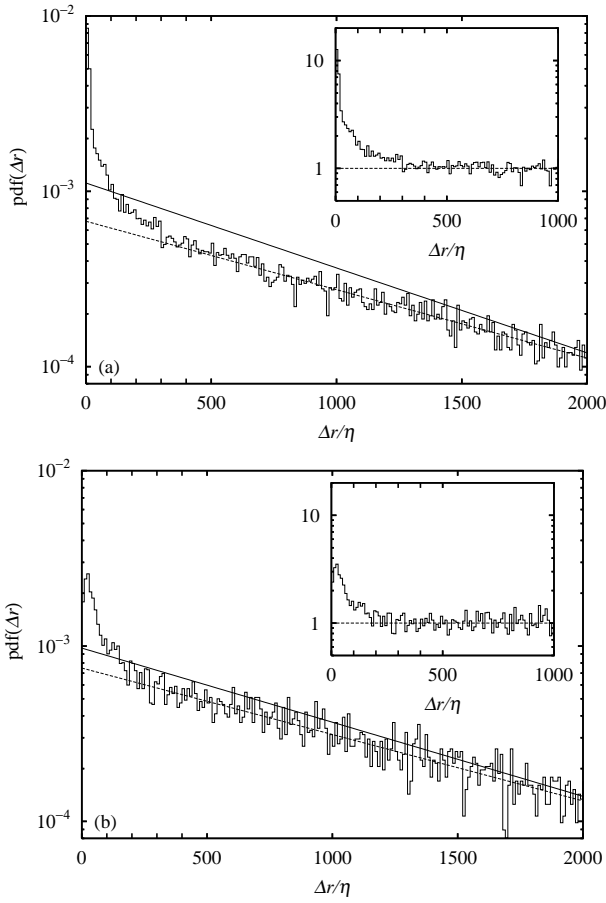


FIG. 2: Probability density function of distance between successive bubbles, $\text{pdf}(\Delta r)$. Exponential behavior, $\rho e^{-\rho \Delta r}$, (solid line) and exponential fit, $A \cdot e^{-\rho_h \Delta r}$, of the large-scale tail (dashed line) are reported. The inset shows the $\text{pdf}(\Delta r)$ compensated by the fitted large-scale exponential behavior, i.e. the $\text{pdf}(\Delta r)$ divided by $A \cdot e^{-\rho_h \Delta r}$.

for case (b) ($Re_\lambda \simeq 180$), confirming the trend of stronger concentration in flows with stronger turbulence level. In figure 3 we show the Kurtosis and Skewness behavior, evaluated for the two cases (a)-(b), in a comparison with the Poissonian dependence. We observe in both cases a clear departure at small scale from the scaling implied by the global homogeneity, this behavior is then recovered at the large scale ($\gtrsim L_0 \simeq 500\eta$) where the data points falls roughly parallel to the Poisson line. The departure from the Poisson line, that is noticeable already at the scales immediately above Δr_{min} , is an indication that bubbles form clusters even at the smallest scale we are able to detect, that is even below 5η for case (a) or 3η for case (b). We observe that for the less turbulent case, (b), the departure from the homogeneous scaling is less marked. A comparison with synthetic Poisson samples of an equivalent number of bubbles, that we have tried, shows that although limited, the available statistics is

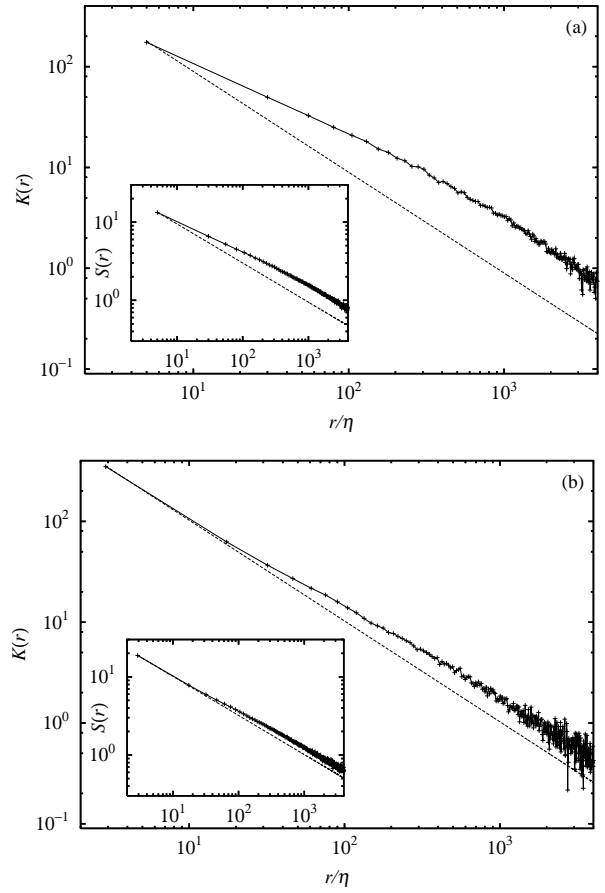


FIG. 3: Scale dependent Kurtosis, $K(r)$, for case (a) (top) and (b) (bottom). Dotted lines represent the Poissonian behavior, that is $K_{(P)}(r) = (\rho r)^{-1}$. Notice that the Poisson scaling behavior is reached for large r -windows only scaling wise. In the insets the scale dependent Skewness, $S(r)$, behavior is shown. Again the Poissonian relation is drawn $S_{(P)}(r) = (\rho r)^{-1/2}$ (dotted line).

enough to validate the deviations from the homogeneity discussed so far. Scale dependent deviation from Poisson distribution is an evidence of the fact that the dispersed microbubbles are trapped within the dynamical vortical structures of turbulence. Furthermore, we observe that gravity plays a minor role in this dynamics. In fact, on average the bubbles are swept down by the mean flow and $g\tau_b/u_\eta \sim O(1)$ (see Tab. I), which implies that even the smallest vortical structures of the flow may trap bubbles [4]. Therefore, it is mainly the inertia that drives the bubble accumulation in the flow.

RESULTS OF THE ANALYSIS ON NUMERICAL DATA

To give an extra support to the interpretation and to the robustness of the analysis that we suggest we do here test the same observables on numerical simulations data.

We do employ standard numerical tools already described and discussed in details in [15, 16]: essentially, we do integrate Lagrangian point-wise bubbles evolved in the background of an Eulerian turbulent field numerically solved by means of a pseudo-spectral method with full 2/3-rule dealiasing.

The equation for the evolution of the point-wise bubble is the following:

$$\frac{d\mathbf{v}}{dt} = 3\frac{D\mathbf{u}}{dt} - \frac{1}{\tau_b}(\mathbf{v} - \mathbf{u}) - 2\mathbf{g} - (\mathbf{v} - \mathbf{u}) \times \boldsymbol{\omega} \quad (1)$$

where \mathbf{u} and $\boldsymbol{\omega}$ are respectively the fluid velocity and vorticity computed at the bubble position and constitute a simplified version of the model suggested in [21]. The Eulerian flows is a turbulent homogenous and isotropic field integrated in a periodic box, of resolution 128^3 , seeded approximately with 10^5 bubbles, corresponding to a void fraction $\alpha = 4.5\%$. Since previous experimental and numerical studies [14, 15] have revealed that the effect of bubbles on strong unbounded turbulence is relatively weak, our numerical bubbles are only coupled in one-way mode to the fluid, i.e. bubbles do not affect the fluid phase. The bubble-Reynolds number Re_b is set to unity and the Stokes number is $St \ll 1$. Therefore, the bubble radius is of order η , and the bubble terminal velocity $v_T = 2g\tau_b$ in still fluid is smaller than the smallest velocity scale u_η . As (and actually more than) in the experiment, the role of gravity is marginal. In Table II we report details of the numerical simulations, these are chosen trying to match the experimental numbers, however we could not reach the same scale separations as in the experiments. In the bottom panel of Tab.II we translated the numerical units to their physical equivalent. We note that in the numerics the Stokes number, $St = \tau_b/\tau_\eta$, which is an indicator of the degree of bubble interaction with turbulence, can not be as low as in the experiments, these would call for extremely high time demanding computations. For practical reason the Stokes values adopted in our numerics are roughly one order of magnitude larger than in the experiments, although always much smaller than unity, $St \ll 1$. Under this conditions, a simple spatial visualizations do show strong bubble accumulation in nearly one-dimensional elongated structures in correspondence to high enstrophy regions (identified as vortex filaments [22]). As already stated, our goal is to use the numerics to confirm the behaviour of the suggested observables. To this end, we put 128 virtual pointwise probes in the flow and recorded the hitting time of bubbles (we give to the bubbles a virtual radius, R_0). In physical reality the bubble radius is related to the bub-

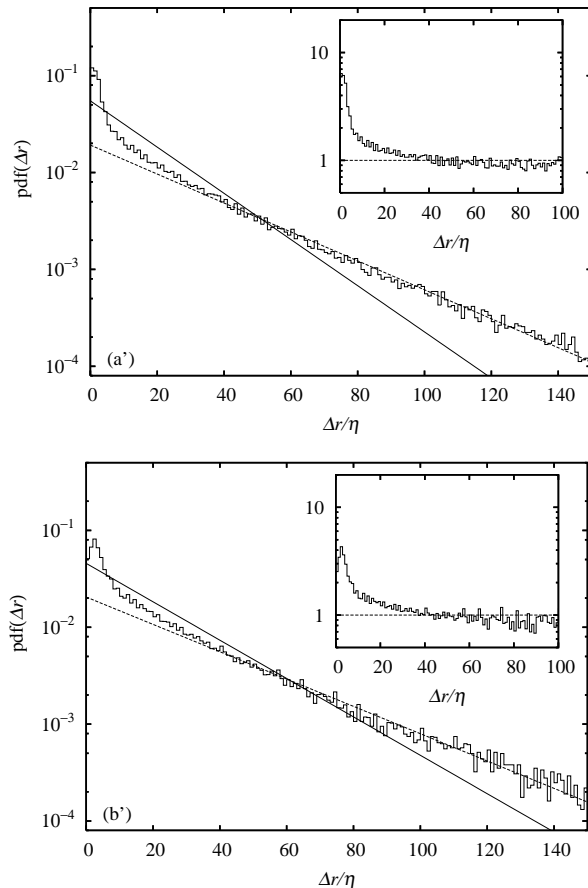


FIG. 4: Numerical result on the probability density function of distance between successive bubbles, $\text{pdf}(\Delta r)$. Case (a') (top) is the most turbulent. In the inset the same compensated plot as in Fig. 2

ble response time, τ_b , via the relation $R_0 \equiv (9\tau_b\nu)^{1/2}$ (supposing no-slip boundary conditions at the gas-liquid interface).

An important difference between the experiments and the numerics is the mean flow: active in the experiment while intrinsically suppressed in the simulations. In the numerical simulations the time is connected to space displacements by mean of the relation $\Delta R = \Delta t \cdot u'$, where, u' , is the root mean square velocity. The level of turbulence, given the available resolution, has been pushed as high as possible ($Re_\lambda \simeq 90$) to obtain a better analogy with the experiment. Furthermore also in the numerics two cases are considered, we vary the amplitude of the external forcing while we keep the bubble size constant, see again Table II.

We show in Figures 4 and 5 the results of the statistical analysis of clustering from the time series obtained from the numerical virtual probes. These two figures should be compared with the analogous experimental findings already discussed and shown in Figures 2 and 3. Some

	L_0	u'	Re_λ	τ_{eddy}	τ_η	η	u_η	Re_b	R_0/η	St	$g\tau_b/u_\eta$
(a')	5.0	1.4	94	3.6	0.093	0.025	0.275	1.0	1.13	0.14	0.55
(b')	5.0	1.0	87	4.9	0.147	0.032	0.218	1.0	0.89	0.09	0.69
	L_0 (cm)	u' (cm/s)	Re_λ	τ_{eddy} (ms)	τ_η (ms)	η (μm)	u_η (cm/s)	Re_b	R_0/η	St	$g\tau_b/u_\eta$
(a')	0.41	7.2	94	57.3	4.7	68.7	1.45	1.0	1.13	0.14	0.55
(b')	0.46	5.5	87	82.5	7.3	85.7	1.16	1.0	0.89	0.09	0.69

TABLE II: Relevant turbulent scales and bubble characteristics for the two numerical simulation performed. The top part reports the actual values in numerical units from the simulation, the bottom part shows for comparison the corresponding physical equivalent quantities for air bubbles in water, this is to better appreciate similarities/differences with the experimental conditions of Table I. The values on the bottom part are computed starting from the dimensionless quantities Re_λ , Re_b , St , and by assuming $\nu = 10^{-6} m^2 s^{-1}$ and $g = 9.8 m s^{-2}$.

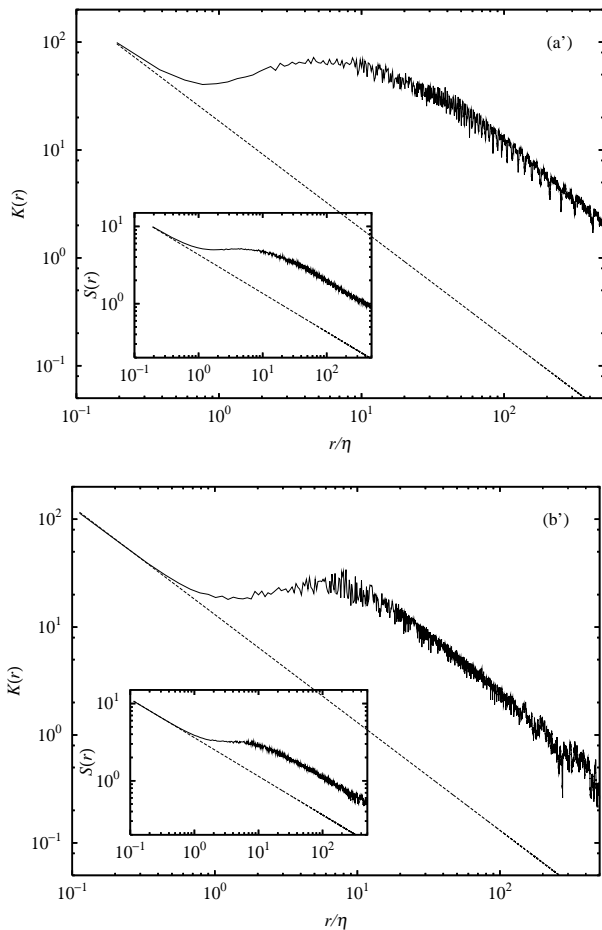


FIG. 5: Numerical result on scale dependent Kurtosis, $K(r)$, for case (a') (top) and (b') (bottom), and Poissonian behavior (dotted). In the insets the scale dependent Skewness, $S(r)$, behavior is shown.

qualitative similarities are striking. First, starting from Fig. 4, we observe that deviations from random and homogeneous, i.e. pure exponential behavior, are relevant at small scales. This feature is confirmed by the scale

dependent Kurtosis and Skewness of Fig. 5, where departure from the Poisson scaling already starts below η scale. Second, the most turbulent case is the most clustered, (a') ($Re_\lambda \simeq 94$) more than (b') ($Re_\lambda \simeq 87$). The evaluation of the fraction of clustered bubbles, based on the fit of the pdf(Δr) as in the experiment, gives the value 29% for (a') and 37% for (b'). Nevertheless, even if the qualitative behavior of the statistical indicators adopted are the same, important differences arise in this comparison and they shall be discussed too. Full homogeneity in the numerics seems to be recovered at scales of order $\mathcal{O}(10\eta)$, this is not the case in the experiments where we reach $\mathcal{O}(100\eta)$ scales, furthermore the deviations from Poisson distribution and the fraction of clustered bubbles are definitely stronger in the numerics. There is more than one possible interpretation for this mismatch. Here we would like to mention what we consider more relevant (besides the possible incompleteness of the model). We first note that some known physical effects have been neglected so far: the fluid-bubble and the bubble-bubble couplings and the associated finite size effects (in the present conditions bubbles can overlap!). A second reason can be the different degree of bubble interaction with turbulence, a quantity that is parametrized by the Stokes number $St = \tau_b/\tau_\eta$. The estimated St in the experiment is roughly one order of magnitude smaller than in the simulation, this corresponds to bubbles that react faster to the fluid velocity changes and hence to bubbles that follow closely the fluid particles and accumulate less. Such a trend is also confirmed by our numerics.

CONCLUSIONS

We have performed statistical tests in order to detect and quantitatively characterize the phenomenon of bubble preferential concentration from single-point hot-wire anemometer measurements in the bulk of a turbulent channel. Our tools clearly shown that the experimental records display bubble clustering. The fraction of bubbles trapped in such structures is indeed relevant

and can be estimated to be of the order of 10%. The scale-dependent deviations from random homogeneous distribution, that we associate to typical cluster dimension, extends from the smallest detectable scale, $\mathcal{O}(\eta)$, to scales in the low inertial range, $\mathcal{O}(100\eta)$. Accumulation of bubbles is enhanced by increasing the turbulence intensity. Comparison with present Eulerian-Lagrangian simulations, where point-like bubbles strongly accumulate in vortex core regions, shows similar qualitative features and trends.

We hope this work will stimulate new dedicated experiments to further quantify the clustering dynamics at changing turbulence intensity and bubble concentration. For instance, an analysis on the statistics of fluid velocity signal just before a bubble arrives on the probe could be interesting to determine the influence of the lift force on the bubble spreading. In fact it is thought that, due to the combined effect of buoyancy and lift, bubbles shall accumulate preferentially in down-flow sides of vortices, [16]. Unfortunately, a corresponding analysis of our experimental data has hitherto not been successful, presumably due to flow contaminations by small impurities.

Finally, we note that the proposed methodology may also be employed to locally quantify the bubble (or particle) clustering in inhomogeneous flows, as for instance in the proximity of jets [23], where the persistence of flows structures makes the preferential concentration an inherent spatial dependent phenomenon.

Acknowledgment: We thank Stefan Luther and Ger-
tWim Bruggert for extensive help with the experimental setup and the measurements, and Kazuyasu Sugiyama for useful discussions. The work is part of the research program of the Stichting voor Fundamenteel Onderzoek der Materie FOM, which is financially supported by the Nederlandse Organisatie voor Wetenschappelijk Onderzoek NWO.

- [2] M. Maxey, *J. Fluid Mech.* **174**, 441 (1987).
- [3] K. Squires and J. Eaton, *Phys. Fluids A* **3**, 1169 (1991).
- [4] L. Wang and M. Maxey, *J. Fluid Mech.* **256**, 27 (1993).
- [5] J. Bec, L. Biferale, G. Boffetta, A. Celani, M. Cencini, A. Lanotte, S. Musacchio, and F. Toschi, *J. Fluid Mech.* **550**, 349 (2006).
- [6] G. Falkovich and A. Pumir, *Phys. Fluids* **16** (2004).
- [7] T. Elperin, N. Kleeorin, M. A. Liberman, V. S. Lvov, and I. Rogachevskii, *Environ. Fluid Mech.* **7**, 173 (2007).
- [8] N. Mordant and J. F. Pinton, *Eur. Phys. J. B* **18**, 343 (2000).
- [9] W. Shew, S. Poncet, and J. F. Pinton, *J. Fluid Mech.* **569**, 51 (2006).
- [10] C. Veldhuis, A. Biesheuvel, L. van Wijngaarden, and D. Lohse, *Nonlinearity* **18**, C1 (2005).
- [11] J. Magnaudet and I. Eames, *Ann. Rev. Fluid Mech.* **32**, 659 (2000).
- [12] S. Douady, Y. Couder, and M. Brachet, *Phys. Rev. Lett.* **67**, 983 (1991).
- [13] J. M. Rensen, S. Luther, and D. Lohse, *J. Fluid Mech.* **538**, 153 (2005).
- [14] T. van den Berg, S. Luther, and D. Lohse, *Phys. Fluids* **18**, 038103 (2006).
- [15] I. Mazzitelli, D. Lohse, and F. Toschi, *Phys. Fluids* **15**, L5 (2003).
- [16] I. Mazzitelli, D. Lohse, and F. Toschi, *J. Fluid Mech.* **488**, 283 (2003).
- [17] S. Luther, J. Rensen, T. van den Berg, and D. Lohse, *Experimental thermal and fluid science* **29**, 821 (2005).
- [18] J. M. Rensen, S. Luther, J. de Vries, and D. Lohse, *Int. J. Multiphase Flow* **31**, 285 (2005).
- [19] R. Zenit, D. Koch, and A. Sangani, *J. Fluid Mech.* **429**, 307 (2001).
- [20] W. Feller, *An Introduction to Probability Theory and Its Applications* (John Wiley, New York, 1968).
- [21] M. Maxey and J. Riley, *Phys. Fluids* **26**, 883 (1983).
- [22] T. H. van den Berg, S. Luther, I. M. Mazzitelli, J. M. Rensen, F. Toschi, and D. Lohse, *J. Turbul.* **7**, 1 (2006).
- [23] M. Campolo, M. V. Salvetti, and A. Soldati, *AIChE J.* **51**, 28 (2005).

[1] J. Fessler, J. Kulick, and J. Eaton, *Phys. Fluids* **6**, 3742 (1994).